fractal and fractional

MDPI

Article

Cardiovascular Circulatory System and Left Carotid Model: A Fractional Approach to Disease Modeling

José Emilio Traver [1,*], Cristina Nuevo-Gallardo [1,*], Inés Tejado [1], Javier Fernández-Portales [2], Juan Francisco Ortega-Morán [3], J. Blas Pagador [3] and Blas M. Vinagre [1]

[1] Escuela de Ingenierías Industriales, Universidad de Extremadura, 06006 Badajoz, Spain; itejbal@unex.es (I.T.); bvinagre@unex.es (B.M.V.)
[2] Hospital San Pedro de Alcántara, 10071 Cáceres, Spain; portales70@hotmail.com
[3] Centro de Cirugía de Mínima Invasión Jesús Usón, Ctra. N-521 km 41.8, 10071 Cáceres, Spain; jfortega@ccmijesususon.com (J.F.O.-M.); jbpagador@ccmijesususon.com (J.B.P.)
* Correspondence: jetraverb@unex.es (J.E.T.); cnuevog@unex.es (C.N.-G.)

Abstract: Cardiovascular diseases (CVDs) remain the leading cause of death worldwide, according to recent reports from the World Health Organization (WHO). This fact encourages research into the cardiovascular system (CVS) from multiple and different points of view than those given by the medical perspective, highlighting among them the computational and mathematical models that involve experiments much simpler and less expensive to be performed in comparison with in vivo or in vitro heart experiments. However, the CVS is a complex system that needs multidisciplinary knowledge to describe its dynamic models, which help to predict cardiovascular events in patients with heart failure, myocardial or valvular heart disease, so it remains an active area of research. Firstly, this paper presents a novel electrical model of the CVS that extends the classic Windkessel models to the left common carotid artery motivated by the need to have a more complete model from a medical point of view for validation purposes, as well as to describe other cardiovascular phenomena in this area, such as atherosclerosis, one of the main risk factors for CVDs. The model is validated by clinical indices and experimental data obtained from clinical trials performed on a pig. Secondly, as a first step, the goodness of a fractional-order behavior of this model is discussed to characterize different heart diseases through pressure–volume (PV) loops. Unlike other models, it allows us to modify not only the topology, parameters or number of model elements, but also the dynamic by tuning a single parameter, the characteristic differentiation order; consequently, it is expected to provide a valuable insight into this complex system and to support the development of clinical decision systems for CVDs.

Keywords: cardiovascular system; electrical model; experimental validation; fractional model; heart diseases; pressure–volume loops

Citation: Traver, J.E.; Nuevo-Gallardo, C.; Tejado, I.; Fernández-Portales, J.; Ortega-Morán, J.F.; Pagador, J.B.; Vinagre, B.M. Cardiovascular Circulatory System and Left Carotid Model: A Fractional Approach to Disease Modeling. *Fractal Fract.* **2022**, *6*, 64. https://doi.org/10.3390/fractalfract6020064

Academic Editors: Norbert Herencsar and Manuel Duarte Ortigueira

Received: 30 November 2021
Accepted: 20 January 2022
Published: 26 January 2022

1. Introduction

Cardiovascular diseases (CVDs) remain the leading cause of death worldwide, according to recent reports from the World Health Organization (WHO). Moreover, its upward trend over the last thirty years continues to increase for almost all countries [1]. In 2019, over 18 million people died from CVDs, which represents 32% of all global deaths; more specifically, 85% of them were due to heart attack and stroke [2]. This fact has encouraged research into cardiovascular system (CVS) models, where experiments involving computational and mathematical models are much simpler and less expensive to be performed in comparison with in vivo or in vitro experiments.

The CVS is a relatively complex system that needs knowledge from several branches of physics and chemistry to understand all its behavior, which has led to the development of models or simulators, in greater or lesser detail, to achieve a global understanding of its

operation. In this respect, numerous models have been proposed and approached from different perspectives, such as from the study of neuroregulation mechanisms, gas exchange or the hemodynamics of the system; however, the latter approach has always received greater attention due to its possible physiological or clinical applications [3,4]. For such an approach, the main methodologies used are: (1) lumped parameter models, which describe, in a simplified manner, the predominant behavior of each of the components involved in the CVS [3,5–9]; (2) distributed parameter models, describing the CVS by one, two or three dimensions based on finite element software [10–12]; or (3) modeling from a hydraulic approach [13–15]. Especially, the three dimensional distributed parameter models have received a great deal of attention in recent decades as a result of the increase in computing power, but these models are more complex and focus on partial vascular zones, and consequently they need longer simulation time and simpler models to define their boundary conditions [16–19].

The models offer the possibility to diagnose or predict the behavior of the CVS when a patient suffers a cardiovascular dysfunction or pathology [20–24], or to study the performance of auxiliary devices [3,25,26]. This reduces the diagnostic time for certain pathologies or research time of functional evaluation of devices under development, while reducing animal experimentation. Nevertheless, the existing models have use limitations in clinical practice due to both their physical and computational complexities. Modeling of pathologies, or even medical assistance devices, usually requires to modify numerous parameters of the model, which are strongly related to each other, making it necessary sometimes to perform new validations. This fact makes the models with a great number of parameters undesirable for real applications. In this regard, lumped parameter models offer an advantage over the others, demonstrating a higher accuracy to execution time ratio, which is suitable for real-time simulations and applications [27,28]. Despite this, lumped models are reduced to describe the main arteries of the CVS [3,5,9,22] or the entire circulatory system [29], complicating the study of certain vascular areas due to a greater number of parameters. This is the case of the carotid artery, for which there are no studies that model its behavior simply and accurately. In spite of this, it is one of the main arteries affected by stenosis according to clinical studies [30].

In what CVD modeling concerns, it is mainly based on the development of new models or the adjustment of numerous parameters to describe a dysfunction or disease accurately. New models require the inclusion of new terms for a better description of the dynamic system or, in the case of parameter adjustment, they can achieve a dynamic similar to the desired one but do not describe it in an accurate way, although it has the advantage of not incorporating new terms. When the CVS suffers a disease, such as stenosis, not only the vessel presents an obstruction, but the calcification of the lumen also has an impact on the elastance, among other properties; therefore, a disease implies an alteration of the system properties, which leads the system to exhibit a different behavior and not only a modification of the resistance or flow capacity. In this regard, fractional calculus can be an adequate tool to describe CVDs. Fractional calculus is a branch of mathematics that deals with non-integer- order derivatives and integrals, and has emerged as an efficient and powerful mathematical tool not only for accurate modeling of many complex phenomena that can be found in several fields of science and engineering, but also for obtaining adequate exploitable models with few parameters [31,32]. Notably, numerous studies have shown that fractional calculus provides a better description of the viscoelastic behavior of the arterial vessel [33–38], as well as for modeling of pathologies, such as tumors [39,40].

Given this motivation, the contributions of this paper are twofold. Firstly, a novel electrical model of the CVS is presented. It extends the classical Windkessel model of four elements to the left common carotid artery, motivated by the need to have a more complete model from a medical point of view for validation purposes, as well as to describe other cardiovascular phenomena in this area, such as atherosclerosis, one of the main risk factors for CVDs. This model is validated with experimental data obtained from clinical trials performed on a pig and clinical indices. Secondly, a new approach is introduced for

CVD modeling based on fractional calculus. To do so, the CVS is analyzed as a complete fractional dynamic system; i.e., the relationship between pressure and flow for arteries or chambers is described with fractional behavior. In this sense, a general model is created, able to describe hemodynamic change due to pathologies, such as loss of elasticity or contractile capacity and not only due to vessel occlusion or valve or heart dysfunction. Specifically, the case of aortic valve stenosis will be discussed describing the proposed model with fractional dynamics and how the order of the system allows us to describe the CVS from a healthy state to a severe degree of stenosis. As an advantage for pathology modeling, the model parameters can be identified and validated for the healthy state and remain constant, with only slight variations as in the real system. Preliminary results of this work can be found in [41,42].

The paper is organized as follows. The functioning of the CVS is briefly explained in Section 2. Section 3 justifies the use of electrical analogies for the description of CVS and describes the CVS model. Section 4 compares and validates the presented model with clinical indices and experimental data. Section 5 provides a discussion of how fractional calculus may be an adequate tool for CVD modeling. Finally, conclusions and future works are drawn in Section 6.

2. Cardiovascular System

This section is devoted to the description of the CVS from a functional point of view, with special attention to the carotid artery. The cardiac cycle is explained through the left ventricular pressure–volume (PV) loops, diagrams that also allow the identification of dysfunctions affecting the CVS. Finally, the most frequent valve pathologies are briefly described.

2.1. Anatomy and Physiology of the CVS

The CVS can be simply described as a distribution network of blood vessels that supplies blood to all the parts of a body thanks to the heart, which performs as a pump. The path followed by the blood is a closed loop, starting in the heart, continuing through the arteries, passing through the capillaries, where the exchange of substances takes place and returning to the heart via the veins. From a functional point of view, the distribution network is divided into two stages: (1) systemic circulation, which transports the oxygen and substances; and (2) pulmonary circulation, which is responsible for the oxygenation of the blood [43].

The heart, responsible for pumping the blood, is composed of a double atria-ventricle chamber, where the ventricle is the pump and the atria is a preloaded chamber. The compression or contraction of the ventricle generates the necessary pressure to inject blood through the arteries. Specifically, the right side pumps the blood into the pulmonary artery, which carries it to the lungs, and then it returns to the left side that pumps it again to the rest of the body. It should be noted that the blood only flows in one way because one-way valves are situated between the chambers to prevent reflux, called atrioventricular valves, and at the output of the ventricles, called semilunar valves.

Regarding the systemic circulation, it begins in the ascending aorta, branching into smaller arteries until it reaches the capillaries, covering the entire body. The main branches are: (1) right and left subclavian arteries, supplying blood to the thorax, head, neck, shoulder and arms; (2) right and left common carotid arteries, carrying blood to the head and neck; and (3) descendent aorta, which continues to the abdominal aorta. Finally, the return path is composed of veins that converge in the vena cava, which ends in the heart. Within the systemic circulation, the carotid arteries stand out for their high incidence of strokes [44].

2.2. Cardiac Cycle and Pressure–Volume Loops

The contraction of the heart is a result of a succession of electrical and mechanical phenomena that occur during a heartbeat, known as the cardiac cycle [43]. The cardiac

cycle is divided into two alternate phases: diastole (dilation period) and systole (contraction period), arranged and simplified in four stages. The cardiac cycle starts with the chambers relaxed and the ventricles partially loaded, and proceeds as follows:

(1) The first stage is the atrial systole and ventricular diastole, in which the atrium contracts, filling the ventricles;

(2) The second stage is atrial diastole and the beginning of ventricular systole, which means that the atrium relaxes until the next cardiac cycle while the ventricles contract and the atrioventricular valves close, increasing the pressure but not achieving enough pressure to open the semilunar valves;

(3) The third stage is the end of ventricular systole, when ventricle pressure rises until it exceeds arterial pressure, opening the semilunar valves and ejecting the blood into the pulmonary and systemic circulation;

(4) The last stage is the ventricular and atrial diastole, when the pressure in ventricles decreases rapidly and all the chambers are passively loaded due to their relaxation. Then, a new cycle starts with the atrial systole.

A graphical way to describe and characterize the cardiac cycle is by means of a left ventricle PV loop, which represents the left ventricular pressure (LVP) versus the left ventricular volume (LVV) throughout the four stages, allowing us to identify changes in heart function, such as preload and afterload factors and contractility of the heart [45]. Another advantage of PV loops is that they allow rapid detection of CVDs, such as heart failure, myocardial and valve diseases. An example of a PV loop is shown in Figure 1, where the different stages of a cardiac cycle corresponding to the left ventricle (LV) are represented from a thermodynamic point of view:

(1) Passive filling (referred to as A-B);
(2) Isovolumetric contraction (denoted as B-C);
(3) Ejection (C-D);
(4) Isovolumetric relaxation (D-A) [46].

Furthermore, these diagrams also provide information on a wide range of variables, such as those listed in Table 1.

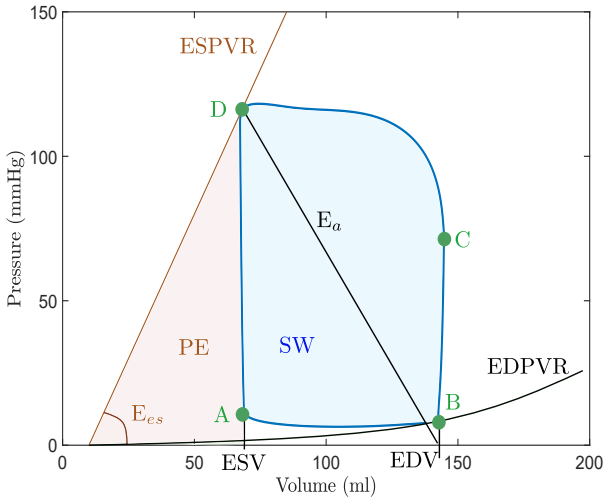

Figure 1. Example of PV loop and parameters that can be measured. The meaning of acronyms are detailed in Table 1. Image adapted from [46,47].

Table 1. Parameters measured from PV loops. Data extracted from [46].

Abbreviation	Parameter	Meaning
EDV	End-diastolic volume	Left ventricular volume in diastole.
ESV	End-systolic volume	Left ventricular volume in systole.
ESPVR	End-systolic PV relationship	Maximal pressure of left ventricle.
EDPVR	End-diastolic PV relationship	Left ventricular pressure in diastole.
E_{es}	End-systolic elastance	Peak chamber elastance during a beat.
E_a	Effective arterial elastance	Relates EDP and EDV to ESV.
SV	Stroke volume	The difference between ESV and EDV.
SW	Stroke work	The area within the loop.
PE	Potential energy	The area within the loop and ESPVR.
PVA	Pressure–volume area	Sum of SW and potential energy PE.
ME	Mechanical efficiency	The ratio between SW and PVA.

With respect to the factors affecting the functioning of the heart, the preload factors refer to the level of distension of the ventricle during diastole, and are proportional to end-diastolic volume (EDV) [43,48]. According to Frank–Starling's law, an increase in ventricular preload leads to an increment of stroke volume (SV), which implies an increase in EDV and the opening pressure of the semilunar valves. These effects are shown in Figure 2a. An increase in preload is associated to an increment in physical exercise and acceleration of heart rate (HR), while an occlusion of the veins or hemorrhages produce a reduction in preload.

The afterload is related to end-systolic volume (ESV), although preload factors and inotropy also affect it. ESV is the pressure that the ventricle must exert in order to open the semilunar valves and propel the blood. In the PV loops, an increase in afterload involves a reduction in SV and an increment in ESV, which also leads to an increase in the EDV (see Figure 2b). The increase in afterload is usually caused by an increased systemic resistance due to damage of the semilunar valves, stenosis or obstructions in the circulation, as well as a loss of elasticity in the aortic artery.

With respect to inotropy, understood as the capacity of the ventricles to contract, a rise of this factor implies a higher slope of the end-systolic PV relationship (ESPVR) line, represented in Figure 2c. This variation allows to have a higher SV and reduces EDV and ESV. Reduced ability to contract is observed as a consequence of a prolonged state of hypoxia, hyponatremia or hypercapnia.

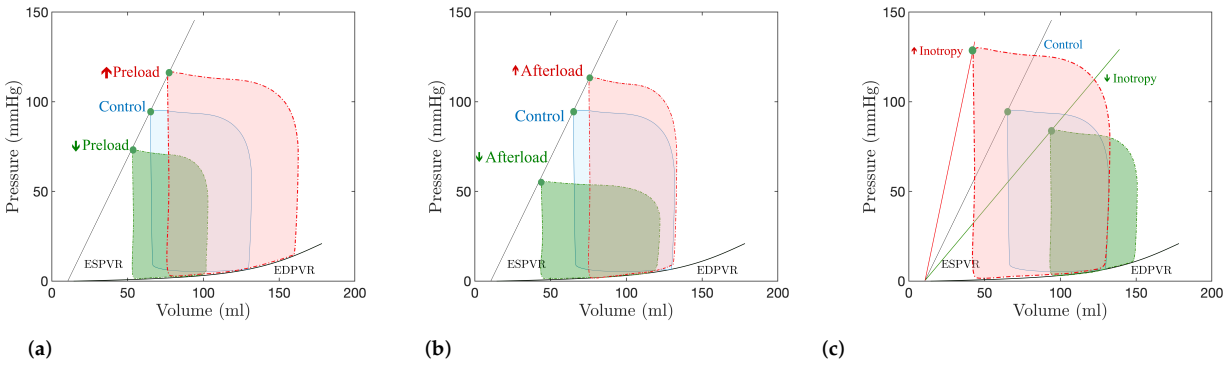

Figure 2. Effects on left ventricular PV diagrams due to changes in: (**a**) preload; (**b**) afterload; (**c**) inotropy.

2.3. Valve Pathologies

The most common valve pathologies are related to the aortic valve and mitral valve, and, in both cases, involve the narrowing of the valve (stenosis) and a defect in the closure.

Stenosis in aortic valve refers to the narrowing of the valve during systole, which can be caused by a congenital abnormality of the valve or progressive calcium buildup on the

valve cups due to age [49]. Conversely, a defect in the closure of the aortic valve leads to a leakage backward into the LV during diastole, and is called aortic valve regurgitation, with similar causes as aortic valve stenosis. In both pathologies, a hypertrophy in the LV appears due to the thickening of the LV muscle to undertake the stress, which causes an increase in LV pressure.

Aortic valve pathologies lead to PV loops with higher amplitude and displaced to the right with respect to the healthy case [46,50,51], as illustrated in Figure 3a,b. The displacement of the loop to the right implies higher values of EDV, ESV and SV, also raising the area within the loop (SW). As SW is higher, the pressure–volume area (PVA) also increases, as it is the sum of SW and potential energy (PE).

With respect to the mitral valve, the pathologies are similar, considering that the leakage is produced during systole from the LV to the left atria (LA). Figure 3c shows that patients with mitral valve stenosis present similar PV loops as a healthy patient, which indicates that this pathology does not affect (to a large extent) the functioning of the LV. On the other hand, patients with mitral valve regurgitation (Figure 3d) present wider PV loops, increasing the afterload and preload and higher amplitude. The shape is slightly different from the healthy case.

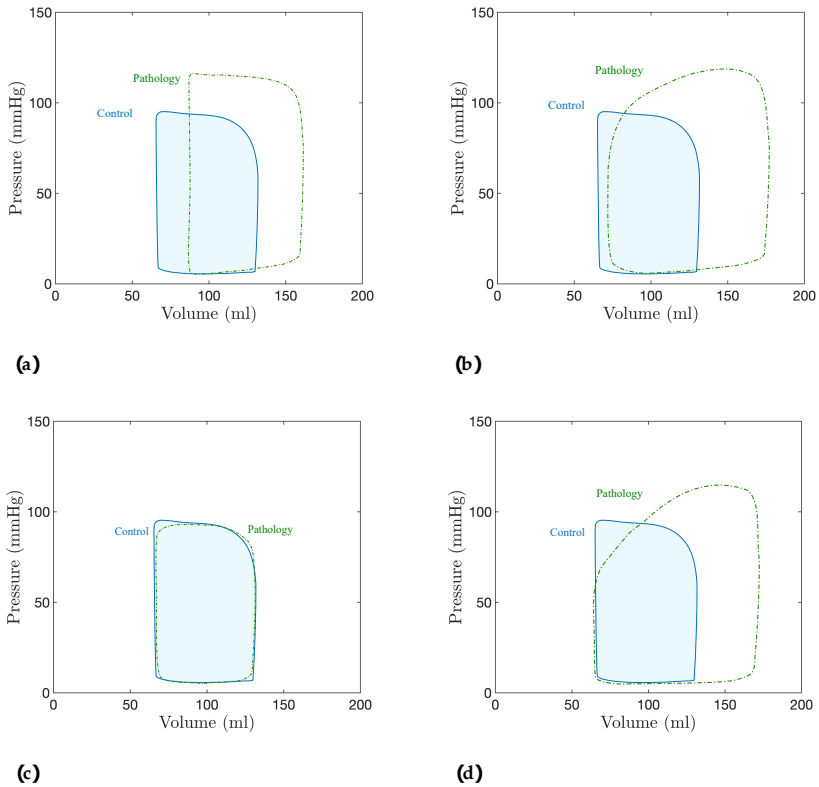

Figure 3. Left ventricular PV loops of different valve pathologies: (**a**) aortic valve stenosis; (**b**) aortic valve regurgitation; (**c**) mitral valve stenosis; (**d**) mitral valve regurgitation.

3. Description of the CVS Model

This section explains the equivalences between the electrical and hydrodynamic indices, allowing us to model the CVS from an electrical point of view. Once the relationships and equivalences between an electrical circuit and the behavior described by a segment of the CVS have been established, the modeling of such a system, as well as the contractile behavior of the heart, are addressed.

3.1. Electrical Equivalences

In order to describe the CVS using a zero dimension (0-D) global parameter model, it is firstly required to understand how it is possible to transfer the fluid dynamics of an

environment to a discrete system, such as electrical circuits. The key concept is to analyze the CVS through segments or compartments, that means defining the relationship between their output and input, which can be calculated either empirically or theoretically.

Applying the Navier–Stokes equations to a blood vessel segment and taking into account the considerations given in [19,52], it is possible to define the relationship between pressure and flow within the segment as:

$$\begin{aligned} K_c l \frac{d\hat{p}}{dt} + q_2 - q_1 &= 0 \\ \frac{\rho l}{A}\frac{d\hat{q}}{dt} + \frac{\rho K_R l}{A^2}\hat{q} + p_2 - p_1 &= 0 \end{aligned} \tag{1}$$

where $\hat{p}$ and $\hat{q}$ are the average segment pressure and flow rate, respectively, p_1 and p_2 and q_1 and q_2 are the pressures and the flow rate at the inlet and outlet, respectively, A denotes the average section of the blood vessel, l is the length of the segment, ρ is the density of the blood, and K_c and K_R are variables dependent on the elastic properties of the blood vessel and the viscosity of the blood (see [4,19] for more information).

The system of Equations (1) implies that the flow and pressure of the segment considered is limited by the boundary conditions ($q_{1,2}$ and $p_{1,2}$). However, the 0-D model does not have boundary conditions, since there is no continuous dependence on space, but rather an input/output relationship; therefore, to solve such a system of equations, it is necessary to establish initial conditions ($p_0 = p_1$ and $q_0 = q_1$) and also to make the following simplifications: $\hat{p} \approx p_2$ y $\hat{q} \approx q_1$. These assumptions, which are valid for relatively short blood vessel segments, result in a 0-D global parameter model [19].

Equations of this type are found in the analysis of resistor–inductor–capacitor (RLC) electrical circuits, which demonstrate the same dynamics [4]. This is shown analyzing the circuit depicted in Figure 4, whose dynamics is defined by the following relationships:

$$\begin{aligned} C\frac{dV_2}{dt} + I_2 - I_1 &= 0 \\ L\frac{dI_1}{dt} + RI_1 + V_2 - V_1 &= 0 \end{aligned} \tag{2}$$

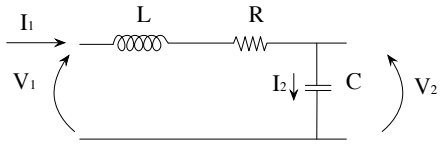

Figure 4. Lumped electrical model equivalent to a short blood vessel segment.

By analogy to an electrical circuit, current represents blood flow, while pressure corresponds to voltage. Likewise, from the sets of Equations (1) and (2) it is possible to establish the equivalence of the electrical components with the variables that define the characteristics of the blood vessel considered as follows: the resistances emulate the opposition of vessel to flow due to viscosity and variation in the diameter of the vessels; the inductance shows the inertial effects that the blood flow experiences as a result of flow variations; and the capacitor represents the conservative term of the principle of mass conservation due to the elasticity of the blood vessels. Assuming that the blood behaves similar to a Newtonian fluid, i.e., a flow developed under a constant pressure gradient, the following definitions of the equivalent electrical components can be written [19]:

$$R = \frac{8\pi\mu l}{A^2}, \qquad L = \frac{\rho l}{A}, \qquad C = \frac{3\pi r^3 l}{2Eh},$$

where μ is the viscosity of the blood, E is the Young modulus and h and r are the thickness and the radius of the vessel, respectively.

3.2. Model

The model on which this work is focused is based on the Windkessel model proposed in [53,54] and the modifications suggested in [3,8,55]. Moreover, this work presents a model that extends the model of [3] to the left common carotid artery. The choice of this kind of artery is motivated by the need to have a more complete model from a medical point of view for validation purposes, as well as to describe other cardiovascular phenomena in this area, such as atherosclerosis, one of the main risk factors for CVDs [30]. It should be also noted that the whole model has been defined based on the anatomic structure of the circulatory system, respecting the criteria used in [54] for the definition of the four element Windkessel model. Then, the equivalent electrical circuit of the CVS and left common carotid artery is shown in Figure 5, where a clear differentiation is made between the systemic circulation dynamic and left carotid dynamic.

The cardiovascular model focuses mainly on the left chambers of the heart, assuming that the right ventricle and the pulmonary circulation act correctly and, hence, they are omitted. Resistance to flow from the descending aorta through the capillary vessels, venous and pulmonary circulation to reach the left atrium is identified through the resistors that feedback the electrical system: R_S denotes the systemic resistance, whereas R_{SLC} represents the resistance from the left common carotid. The contractile capacity of the heart is modeled by the variable capacitor, $C(t)$, whose capacitance is the inverse of the LV elastance ($E(t)$). The last term defines the elasticity of the heart as a function of the pressure that it supports, according to the Frank–Starling's law. A more detailed description is provided in Section 3.3. The aortic and mitral valves are modeled as ideal diodes, D_A and D_M, in series with a resistance, R_A and R_M, respectively. However, to achieve a more accurate response, the capacitor C_A is added to the first valve, which reflects the elasticity of ascending aorta and models the pressure variation due to the open–close operation of the aortic valve. The rest of elements, which are based on the Windkessel model and the anatomical distribution of the circulatory system, model the elasticity, inertia and resistance of the descending aorta (C_S, L and R_C) and the left common carotid artery (C_{LC} and L_{LC}). These elements, in combination with R_S and R_{SLC}, define the afterload factors.

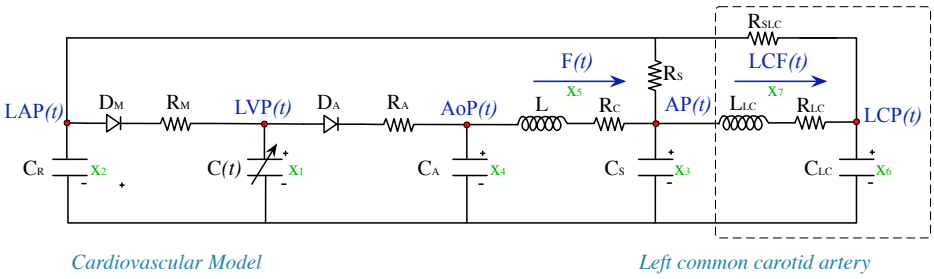

Figure 5. Electrical model equivalent to the CVS with extension to left common carotid artery.

With respect to the dynamics of the CVS, it is described choosing as state variables the ones listed in Table 2 (they correspond to those indicated in Figure 5), and applying Kirchhoffs' laws to the electric circuit, except for the state x_1, which depends on the working mode of the diodes, the contractile capacity of the heart $C(t)$. The diodes allow to define the behavior of heart valves and give the system its non-linear character. The combination of the conduction state of the diodes allows us to describe the four stages of the cardiac cycle, establishing four different equivalent electrical circuits for each stage and, therefore, a set of linear differential equations. This implies a different analysis of the circuit for each of the stages of the cardiac cycle. To overcome this drawback, the diodes are described as a ramp function, $d(x)$, with which the system can be described by a single definition

throughout the entire cardiac cycle. Taking into account these considerations, the complete model can be expressed as:

$$\begin{aligned}
\dot{x}_1 &= \frac{1}{C(t)}\Big(-\dot{C}(t)x_1 + \frac{1}{R_M}d(x_1 - x_2) - \frac{1}{R_A}d(x_4 - x_1)\Big)\\
\dot{x}_2 &= \frac{1}{C_R}\Big(\frac{1}{R_S}d(x_3 - x_2) + \frac{1}{R_{SLC}}(x_6 - x_2) - \frac{1}{R_M}d(x_2 - x_1)\Big)\\
\dot{x}_3 &= \frac{1}{C_S}\Big(x_5 - x_7 - \frac{1}{R_S}d(x_3 - x_2)\Big)\\
\dot{x}_4 &= \frac{1}{C_A}\Big(\frac{1}{R_A}d(x_4 - x_1) - x_5\Big)\\
\dot{x}_5 &= \frac{1}{L}\Big(x_4 - x_3 - R_C x_5\Big)\\
\dot{x}_6 &= \frac{1}{C_{LC}}\Big(\frac{1}{R_{SLC}}(x_2 - x_6) + x_7\Big)\\
\dot{x}_7 &= \frac{1}{L_{LC}}\Big(x_3 - x_6 - R_{LC}x_7\Big)
\end{aligned} \tag{3}$$

Table 2. State variables of the cardiovascular model.

Variable	Abbreviation	Clinical Meaning (Unit)
$x_1(t)$	LVP(t)	Left ventricular pressure (mmHg).
$x_2(t)$	LAP(t)	Left atrial pressure (mmHg).
$x_3(t)$	AP(t)	Descending aorta pressure (mmHg).
$x_4(t)$	AoP(t)	Ascending aorta pressure (mmHg).
$x_5(t)$	F(t)	Total flow (mL/s).
$x_6(t)$	LCP(t)	Left common carotid artery pressure (mmHg).
$x_7(t)$	LCF(t)	Carotid artery flow rate (mL/s).

The detailed analysis of the electrical circuit in Figure 5 can be found in Appendix A. It should be remarked that the above model defines an autonomous switched time-varying system over different phases within the cardiac cycle.

3.3. Elastance

The elastance represents the state of contraction of the LV, relating the pressure and volumes of the LV according to the Frank–Starling's law, which is defined as [3,56]:

$$E(t) = \frac{LVP(t)}{LVV(t) - V_0}, \tag{4}$$

where $LVV(t)$ is the left ventricular volume, whereas V_0 is the reference volume that corresponds to the theoretical ventricular volume at zero pressure.

The definition of elastance was addressed in different studies [57–59], where they tried to adjust it empirically to a standard function. In particular, most of them agree that the definition can be normalized and scaled between the points of maximum and minimum functioning of the LV as:

$$E_H(t) = (E_{max} - E_{min})E_n(t_n) + E_{min}, \tag{5}$$

where E_{max} and E_{min} are constants related to ESV, EDV and ESPVR, and $E_n(t_n)$ is the normalized elastance, with $t_n = t/T_{max}$, $T_{max} = 0.2 + 0.15t_c$, being $t_c = 60/HR$ the time period of the heart cycle. In certain pathologies, the elastance can have the same morphology for a healthy or sick heart [60]. Then, for some cardiac conditions, the elastance model (5) is modified to $E(t) = \delta E_H(t)$, with $0 \leq \delta \leq 1$, where lower values of δ represent

CVDs (the more severe the disease, the lower the value of δ), whereas $\delta = 1$ corresponds to the healthy state.

This work focuses in the definition for elastance provided by [57], which describes it for a healthy person as:

$$E_n(t_n) = C\left(\frac{\left(\frac{t_n}{B}\right)^{\alpha_E}}{1+\left(\frac{t_n}{B}\right)^{\alpha_E}}\right)\left(\frac{1}{1+\left(\frac{t_n}{A}\right)^{\beta_E}}\right) \quad (6)$$

and whose waveforms are depicted in Figure 6. The first term in the brackets describes the ascending part of the curve and the second one, the descending part. The parameter C is the amplitude of elastance, related to the maximum arterial pressure, α_E and β_E denote the ascending and descending slopes through the LV relaxation time, respectively, and A and B are constants to define the relative appearance of each curve within the heart period.

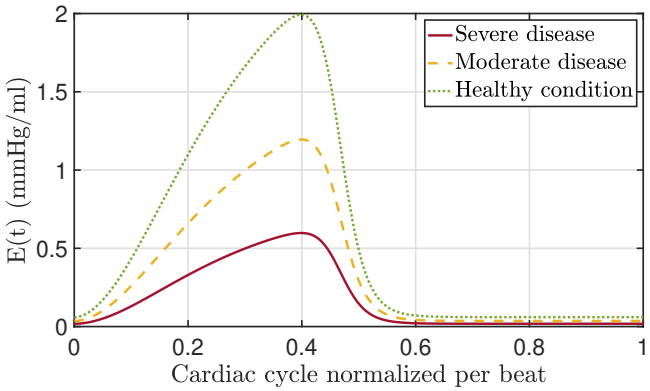

Figure 6. Elastance according to Stergiopulos's work [57]. The parameters used are shown in Table 3.

4. Validation of the CVS Model

This section presents the validations of the above-described CVS model from different points of view. Firstly, the model is validated in terms of both the main hemodynamic indices and the waveform of the main variables in Table 2, comparing the results in a healthy state (nominal condition) with the collected in the bibliography and with experimental data, respectively. Secondly, the consistency of the model is addressed by evaluating the response to variations in the preload and afterload factors. The values of the parameters involved in the CVS for the different simulations are included in Table 3.

4.1. Clinical Parameters and Experimental Waveforms

Next, the model is validated comparing the hemodynamic parameters resulting from the model simulation and those collected in the clinical literature, as well as from experimental data. Hence, this first validation allows us to conclude whether the model provides reasonable and coherent results. Secondly, cardiovascular waveforms corresponding to simulated and experimental data are compared to confirm whether the dynamics is correct.

As for the experimental data, they were obtained from a clinical trial performed on a pig, due to its similarities with human anatomy and hemodynamics. For data collection, the animal was under sedation during the whole process and catheterization methods were used to measure the variables listed in Table 2, with the exception of flow rate, which was measured indirectly by means of cardiac output and the carotid artery flow rate because the specific instrumentation for such measurement was not available. In order to improve the reproducibility of the data and reduce signal noise at the post-processing step, the pressure signals and the cardiac output were collected ten and five times, respectively. To make the experimental data usable, they were previously filtered and, then, synchronized, since all the signals were not collected at the same time, taking for the analysis the mean of the ten repetitions. Data were collected with a sample time of 4 ms.

Table 3. Values of the parameters of the CVS model for validation purposes.

Parameter	Value	Physiological Meaning
	Resistors	
R_S	1	Total peripheral resistance
R_{SLC}	10	Left common carotid peripheral resistance
R_M	0.005	Mitral valve resistance
R_A	0.001	Aortic valve resistance
R_C	0.0398	Characteristic resistance
R_{LC}	10	Left common carotid resistance
	Capacitors	
C_R	8.8	Left atrial compliance
C_S	1.33	Systemic compliance
C_A	0.08	Aortic compliance
C_{LC}	0.09	Left common carotid
	Inductors	
L	0.0005	Inertia of blood in aorta
L_{LC}	0.03	Inertia of blood in left common carotid
	Left ventricle	
E_{max}	2	Maximum volume in diastole
E_{min}	0.06	Minimum volume in diastole
V_0	10	Reference volume at zero pressure (mL)
HR	75	Heart rate (bpm)
	Elastance	
A	1.17	Shape parameter
B	0.7	Shape parameter
C	1.55	Amplitude
α_E	1.9	Ascending slope of the LV relaxation time
β_E	21.9	Descending slope of the LV relaxation time

On the one hand, the main indices used in the literature to describe the hemodynamic status of a patient are listed in Table 4, as well as their range of acceptable values according to the clinical literature [61]. The table also contains the values obtained from the model simulation and the experiments. It can be seen that the indices corresponding to both the model and the experiments are close, consistent and within the range suggested in the literature.

On the other hand, cardiovascular waveforms of the model and the experiments are shown in Figure 7 for a healthy state with the HR given in Table 3. As can be observed, waveforms are consistent as explained next. The systolic LAP coincides with the diastolic LVP. In the case of the model response, the behavior is close to the ideal case. The ascending aorta pressure (AoP) is delayed with respect to LVP as a consequence of the opening and closure of the aortic valve and the propagation of the pressure wave along the artery. In the model, the delay is lower because the AoP is modeled close to the aortic valve, whereas in experiments the pressure sensor was relatively far away from it, the wave propagation time is longer and, consequently, the delay between the LVP and the AoP increases. The same behavior is observed in the left common carotid pressure (LCP); however, small differences can be noticed: the simulated waveforms magnify the pressure fluctuation, especially in the ascending aorta and the LCP, in contrast to the experimental one, where these fluctuations are smoother and the AoP is higher during the systole contraction. It is important to remark that these discrepancies are strongly related to the point at the pressure was measured, obtaining greater or lesser delay and variation in pressure. Likewise, the contraction time is longer in the experimental data.

Regarding the pressure and flow waveforms in the left common carotid artery, the main characteristics that are observed are the following: (1) a time lag with respect to LVP; (2)

a slight increase in pressure; (3) a greater dicrotic wave; (4) a negative flow and a second impulse of blood in ventricular diastole. Again, the differences between the experimental and simulated data are mainly due to the point at which the pressure was measured.

To sum up, the model results are consistent with hemodynamic parameters obtained from the literature and experimental data, concluding that the proposed model is valid and provides results comparable with medical data; however, a larger study with a greater number of tests would allow more accurate results to be obtained.

Table 4. Hemodynamic parameters: comparison between values from literature, proposed model and experiments.

Data from	Heart Rate Pressure (mmHg)	Systolic Arterial Pressure (mmHg)	Diastolic Arterial Pressure (mmHg)	Mean Arterial Pressure (L/s)	Cardiac Output CO (mL/beat)
Literature	50–90	90–140	60–90	70–105	4–8
Model	68	112	77	92	5.90
Experiments	67–70	89	62	68	3.18

Data from	Stroke Volume SV (mmHg)	Systolic LVP (mmHg)	Diastolic LVP (mL)	Max LVV (mL)	Min LVV (mmHg)	Systolic LAP (mmHg)	Diastolic LAP (mmHg)
Literature	60–100	100–140	4–15	77–195	19–72	∼12	∼12
Model	78.71	117	7	137	67	12	7
Experiments	46.83	82	9	–	–	16	10.5

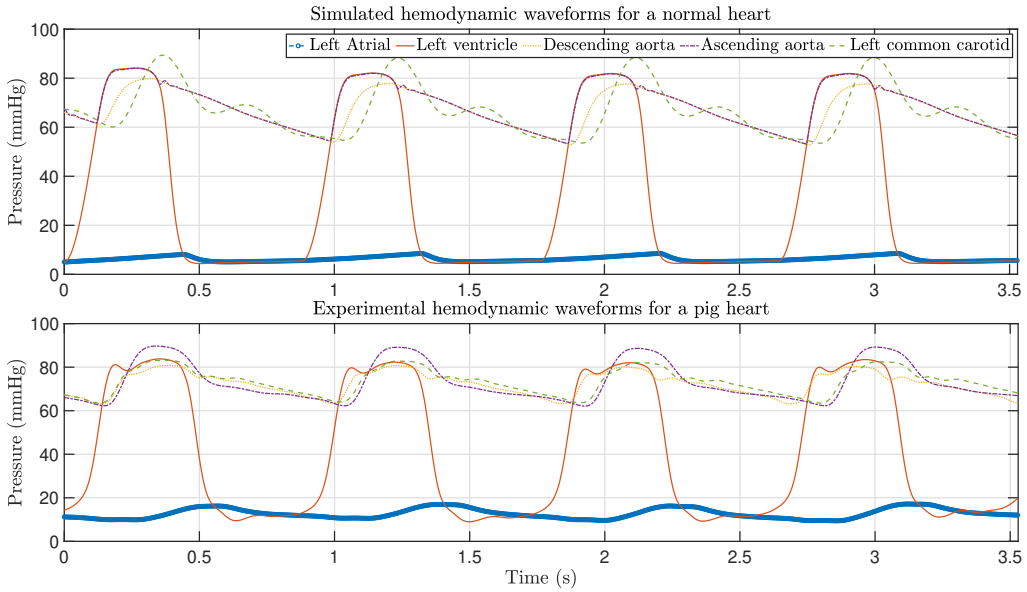

Figure 7. Hemodynamic waveforms of the CVS model (3) compared with experimental data. Experimental data are available in the Supplementary material.

4.2. Preload and Afterload Dynamics

The second method of model validation consists of modifying the components that are related with pre and afterload factors. If the model behaves as expected, the ESPVR determined by E_{max} must be maintained for the different conditions, despite the changes for pre and afterload.

To check this feature, a total of eight pre and afterload conditions, four of each, have been performed and represented in Figure 8 using PV loops. Figure 8a shows the behavior of the model when variations in preload conditions are introduced, in particular by modifying the value of the mitral valve resistance, R_M. The obtained dynamics corresponds with that explained in Section 2: a reduction in the EDV and a slight reduction in the

opening and closure pressures of the semilunar valves is observed. On the other hand, the variation of afterload conditions through the parameter R_S, shown in Figure 8b, results in a reduction in the ejection volume and an increase in the opening and closure pressures of the semilunar valves.

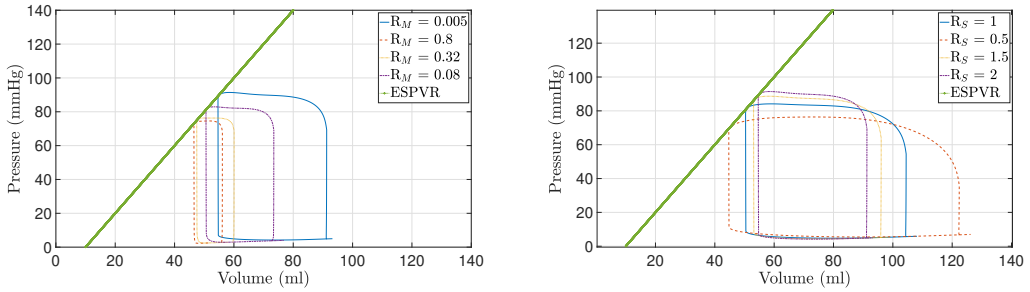

(a) **(b)**

Figure 8. PV diagrams for different pre and afterload conditions: (**a**) variation of preload conditions through R_M; (**b**) variation of afterload conditions through R_S.

Finally, it should be noted that the ESPVR, the line joining the V_0 and ESV points, shows the same slope under all conditions, and its value is consistent with the characteristics of the LV (E_{max} and V_0); therefore, the results confirm the validity of the model to reproduce the dynamics of the CVS and the behavior of the LV under different conditions.

5. Discussion: Modeling of Pathologies

Heart failure is one of the most frequent causes of death in the western world. Improvements in understanding this organ and, by extension, the CVS, may lead to new diagnosis and treatment options for CVDs. As such, this area of research is critical for reducing casualty rates in potentially treatable situations.

In order to study possible CVDs, it is expected that CVS models allow us to simulate and reproduce different kinds of pathologies, including, for example, heart or valve dysfunctions, as well as artery narrowing or occlusion. Among them, this work focuses on valve pathologies, specifically on aortic valve stenosis and regurgitation. The simulation of such pathologies can be achieved by the variation of a large number of parameters, such as elastance, HR and others, which implies a high challenge in terms of estimating the adequate values of these parameters as they need experimental data to be validated. Nevertheless, valve stenosis also involves a variation in the dynamics of some elements of the CVS, and it should not be reflected as a simple lumen obstruction or a modification of parameters of the CVS model. Due to this, the behavior of the real system should be reflected on the model, which can be achieved by the application of fractional calculus, providing a modification in the dynamics of certain elements of the model that could exhibit anomalous behavior. In this way, several properties of these elements, such as the diameter and the elasticity of the vessels, can be modified at the same time. Thus, fractional calculus can help to increase the accuracy of the proposed model and simplify disease modeling.

In this regard, a new approach to CVD modeling based on fractional calculus is presented. The model described in Section 3 is analyzed from the point of view of a system with fractional dynamics, resulting in a system whose dynamics can be modified with a single parameter to describe different conditions, but without changing the rest of its parameters, which have been already validated. As a first step in CVD modeling, the model analysis have been focused on a disease affecting LA compliance, describing the relation between LA volume (LAV) and LA pressure (LAP). Such an anomalous behavior is represented by a fractional relationship between the pressure and flow in the chambers. In the following, the fractional-order model is implemented and simulated in the MATLAB®/ Simulink environment to study how the fractional order could allow to model different pathologies.

5.1. Fractional-Order Model

A dysfunction or anomalous behavior of the CVS is expected to be described by a fractional model, which can be defined in the form:

$$\mathcal{D}^{\alpha} z = f(z) \tag{7}$$

where $\mathcal{D}^{\alpha}$ is the fractional operator of order $\alpha \in \Re^{+}$, $0 < \alpha < 2$, based on Caputo's definition [62], $z \in \Re^{N}$ is a state vector, $f(z) \in \Re^{N}$ is a function vector that models the dynamic of states, and $N \in \aleph$ is the number of states.

In the following, the fractional model is focused on LA compliance, which corresponds to state x_2 and is mainly described by the capacitor C_R in the electrical equivalent circuit. An anomalous operation of this element is modeled as a fractional impedance, and its dynamics is also governed by Ohm's law but applying a fractional operator, as follows:

$$I_2 = C_R \mathcal{D}^{\alpha} x_2,$$

where the differentiation order α allows to describe a fractance, whose behavior varies from a resistor to a capacitor, which, in medical terms, could reflect variation on the volume capacity or the elasticity of LA. Replacing the above fractional behavior on the model described in Section 3 and detailed in Appendix A, the differential equation corresponding to state x_2 is rewritten as:

$$\mathcal{D}^{\alpha} x_2 = \frac{1}{C_R}\Big(\frac{1}{R_S} d(x_3 - x_2) + \frac{1}{R_{SLC}}(x_6 - x_2) - \frac{1}{R_M} d(x_2 - x_1)\Big),$$

while the rest of equations of the CVS model keeps unchanged. The completed model is detailed in Appendix B, where it is also considered that any compliance element may be subject to anomalous behavior.

This new description of the CVS with fractional dynamics makes up a more complete model that allows to describe, not only a healthy state, but also different pathologies and diseases. In this sense, it is not necessary to describe a new topology or parameters of the models, but rather the dynamic by tunning the differentiation order. As we see in the CVS, its elements remain constant with only slight variations, and it is the functionality of the heart, the ventricle or the valves, among others, that is affected.

5.2. Results

For the analysis of CVD modeling, PV loops are used, because a decrease in the capacity of the LA is shown when the LA dilates and its contractility decreases, leading to changes in LA preload and afterload [63,64]. Moreover, it has been demonstrated that LA and LV functions are strongly related, i.e., one is influenced by the other during the cardiac cycle, so changes in LA function can be reflected in PV loops.

The results for values $\alpha \in (0, 1]$, depicted in Figure 9a, show that the ESPVR line remains constant for every value of α, and thus, the contractility is not affected. The afterload and preload increase due to wider and higher loops, respectively. Table 5 shows the obtained values of the parameters indicated in Table 1, representing $\alpha = 1$ the healthy case. Taking into account these results, the values of EDV and ESV increase as the order of the model decreases, as well as the SV. The indices SW, PE, PVA and ME increase in the same way as SV for all the models. For a better comprehension, the error rate between the healthy and the pathological cases, in percentage, has been included in Table 5 in brackets. For values of $\alpha \in [1, 2)$, the model reflects a similar behavior: contractility capacity is maintained, whereas SV increases; however, an increase in pressure in the ESV is also observed. This increase in pressure may be associated with valve or artery occlusion; therefore, the degree of obstruction can be related to the fractional order, where severe states are described with values close to 1.

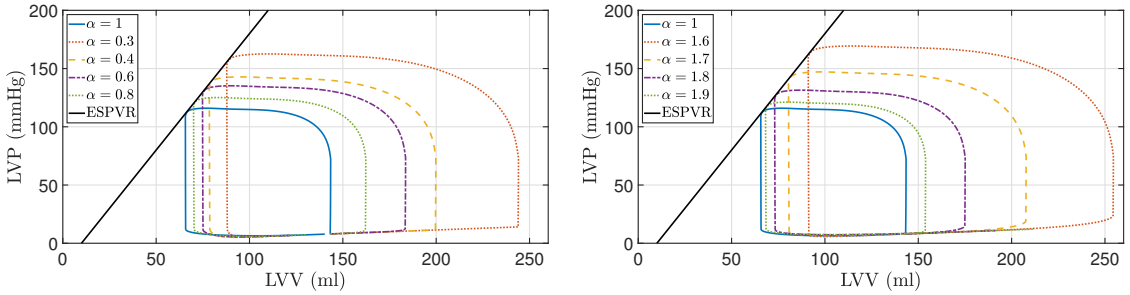

(a) **(b)**

Figure 9. PV loops for state variable x_2 with fractional behavior considering: (**a**) $0 < \alpha \leq 1$; (**b**) $1 \leq \alpha < 2$.

As of the results, the behavior of fractional-order model with $\alpha \in (0, 1]$ shows similarities with patients with aortic valve stenosis or aortic valve regurgitation [46,49–51]. Changes in afterload can be distinguished, related to damage in the valves, stenosis or obstructions in the circulation, as well as a loss of elasticity in the aortic artery, as explained in Section 2.

Table 5. Measurements from PV loops of the electrical model with different fractional-order derivatives, considering only x_2 (extracted from Figure 9). The case $\alpha = 1$ corresponds to a healthy patient.

Model Order		SV (mL)	SW (J/beat)	PE (J/beat)	PVA (J/beat)	ME (%)
Healthy	$\alpha = 1$	**77.69**	**1.03**	**0.38**	**1.42**	**72.92**
$\alpha < 1$	$\alpha = 0.8$	92.01 (18.43%)	1.34 (29.12%)	0.45 (17.27%)	1.79 (25.91%)	74.78 (2.54%)
	$\alpha = 0.6$	108.62 (39.81%)	1.70 (64.14%)	0.52 (37.25%)	2.23 (56.86%)	76.30 (4.63%)
	$\alpha = 0.4$	121.08 (55.85%)	2.00 (92.73%)	0.59 (53.21%)	2.59 (82.03%)	77.21 (5.87%)
	$\alpha = 0.3$	156.01 (100.81%)	2.89 (178.77%)	0.76 (98.46%)	3.66 (157.03%)	79.09 (8.45%)
$\alpha > 1$	$\alpha = 1.9$	85.57 (10.14%)	1.19 (15.22%)	0.42 (9.51%)	1.62 (13.67%)	73.91 (1.35%)
	$\alpha = 1.8$	102.88 (32.42%)	1.54 (48.52%)	0.49 (29.06%)	2.04 (43.23%)	75.60 (3.67%)
	$\alpha = 1.7$	127.03 (63.50%)	2.14 (106.18%)	0.62 (61.81%)	2.76 (94.17%)	77.43 (6.18%)
	$\alpha = 1.6$	163.27 (110.15%)	3.13 (201.88%)	0.83 (115.01%)	3.96 (178.36%)	79.08 (8.44%)

6. Conclusions

The complexity of the cardiovascular system (CVS) has led to the use of equivalent models, most of them with electrical components, that allow us to emulate the behavior of cardiovascular diseases (CVDs) through the modification of numerous parameters, making it possible to perform experiments in a much simpler and less expensive way compared to in vivo or in vitro heart experiments.

This work has presented a novel electrical model of the CVS that extends the classic Windkessel models to the left common carotid artery motivated by the need to have a more complete model from a medical point of view for validation purposes, as well as to describe other cardiovascular phenomena in this area, such as atherosclerosis, one of the main risk factors for CVDs. The extended CVS model was validated using the main clinical indices, and the cardiovascular waveform was compared with experimental data obtained from clinical trials performed on a pig. Likewise, the model showed consistency despite variations in the preload and afterload factors.

On the other hand, as opposed to the traditional approach to CVD modeling based on the development of new models or the adjustment of a wide range of parameters to describe different types of diseases, a completely new perspective was discussed considering that the system has a fractional dynamics. Focusing on the left atria (LA) with a fractional dynamic with order between $(0, 2)$, the results shown hemodynamics similar to those of patients with aortic valve stenosis and aortic valve regurgitation as the order of the model decreases. Thus, it was demonstrated that a fractional calculus approach to model the CVS

allows us to describe a healthy state and CVD at the same time by modifying only the order of the model, where a change of order implies a variation of the system properties.

Our future works will focus on: (1) performing a more detailed study to identify other possible pathologies; (2) applying fractional-order derivatives to other state variables; and (3) validating the pathology models with experimental data.

Supplementary Materials: The following are available online at https://www.mdpi.com/article/10.3390/fractalfract6020064/s1.

Author Contributions: This work involved all coauthors. J.E.T. and C.N.-G. wrote the original draft and contributed to the investigation and the analysis, performed the simulations, edited the manuscript and contributed to the illustrations. J.F.-P. provided support in obtaining the experimental data and validating the model from the medical point of view. I.T. and B.M.V. conceived the idea, contributed to the editing and supervised the manuscript. J.F.O.-M. and J.B.P. provided support in obtaining the experimental data and revised the manuscript. All authors have read and agreed to the published version of the manuscript.

Funding: This work has been supported in part by the Consejería de Economía, Ciencia y Agenda Digital (Junta de Extremadura) under the project IB18109 and the grant "Ayuda a Grupos de Investigación de Extremadura" (no. GR18159), by the Agencia Estatal de Investigación (Ministerio de Ciencia e Innovación) through the project PID2019-111278RB-C22/AEI/10.13039/501100011033, and in part by the European Regional Development Fund "A way to make Europe".

Institutional Review Board Statement: The study was approved by the Ethical Committee of animal experimentation of the Jesús Usón Minimally Invasive Surgery Centre and autorized by the Extremadura Government (Number: EXP-20200518, approved on 20/05/2020). Furthermore, this study was in accordance with the welfare standards based on the FELASA Guidelines.

Informed Consent Statement: Not applicable.

Data Availability Statement: Experimental data associated with this article will be made available on request.

Acknowledgments: José Emilio Traver would like to thank the Ministerio de Educación, Cultura y Deporte its support through the scholarship no. FPU16/2045 of the FPU Program. All authors would like to thank Jesús Usón Minimally Invasive Surgery Centre for offering the possibility of obtaining the data used in this work.

Conflicts of Interest: The authors declare no conflict of interest.

Abbreviations

The following abbreviations are used in this manuscript:

MDPI	Multidisciplinary Digital Publishing Institute
CVD	Cardiovascular disease
WHO	World Health Organization
CVS	Cardiovascular system
PV	Pressure-volume
EDV	End-diastolic volume
ESV	End-systolic volume
ESPVR	End-systolic PV relationship
EDPVR	End-diastolic PV relationship
E_{es}	End-systolic elastance
E_a	Effective arterial elastance
SV	Stroke volume
SW	Stroke work
PE	Potential energy
PVA	Pressure-volume area
ME	Mechanical efficiency
LV	Left ventricle

LA	Left atria
LA	Left atria volume
LVP	Left ventricular pressure
LVV	Left ventricular volume
HR	Heart rate
LAP	Left atrial pressure
AP	Descending aorta pressure
AoP	Ascending aorta pressure
F	Total flow
LCP	Left common carotid artery pressure
LCF	Left common carotid artery flow rate

Appendix A. Integer-Order CVS Model

The mathematical description of the circuit is obtained applying the Kirchoff's circuit law to the electrical circuit depicted in Figure 5 and taking the state variables given in Table 3. With respect to diodes, their behavior is defined by the ramp function:

$$d(x) = \begin{cases} x, & \text{if } x \geq 0 \\ 0, & \text{if } x < 0 \end{cases} \tag{A1}$$

Then, the dynamic equations of the model are obtained as follows. The state x_1 is described recalling the Frank–Starling's law, which states that:

$$E(t) = \frac{LVP(t)}{LVV(t) - V_0}$$

where $LVV(t) = \int (I_M - I_A)dt$ is the charge in the capacitor, being I_M and I_A the currents through the mitral diode D_M and the aortic diode D_A, respectively. Therefore, the state x_1 is defined as:

$$x_1 = E(t)\Big(\int (I_M - I_A)dt - V_0\Big)$$

Deriving the terms on both sides of the equality and recalling that $E(t) = 1/C(t)$ and $\dot{E}(t) = -\dot{C}(t)/C^2(t)$, the differential equation for x_1 can be written as:

$$\begin{aligned} \dot{x}_1 &= \dot{E}(t)\Big(\int (I_m - I_a)dt - V_0\Big) + E(t)\frac{d}{dt}\int (I_M - I_A)dt \\ \dot{x}_1 &= \frac{1}{C(t)}\Big(-\dot{C}(t)x_1 + \frac{1}{R_M}d(x_1 - x_2) - \frac{1}{R_A}d(x_4 - x_1)\Big) \end{aligned} \tag{A2}$$

Applying the Kirchoff's first law to C_R capacitor, it results that

$$I_S = I_2 + I_M$$

where I_S, I_2 and I_M are the currents through the systemic resistance and return from left common carotid, the capacitor C_R and the mitral diode D_M, respectively. Using the Ohm's law, the currents are expressed as a function of voltage:

$$\frac{1}{R_S}(x_2 - x_3) + \frac{1}{R_{SLC}}(x_2 - x_3) = C_R\dot{x}_2 + \frac{1}{R_M}d(x_1 - x_2)$$

Solving for $\dot{x}_2$, it obtains:

$$\dot{x}_2 = \frac{1}{C_R}\Big(\frac{1}{R_S}d(x_3 - x_2) + \frac{1}{R_{SLC}}(x_6 - x_2) - \frac{1}{R_M}d(x_2 - x_1)\Big) \tag{A3}$$

Similarly, the application of Kirchoff's first law to the x_3 node allows obtaining:

$$x_5 = x_7 + \frac{1}{R_S}(x_3 - x_2) + I_3$$

where I_3 is the current through the capacitor C_S. Using the Ohm's law for I_3 and solving for $\dot{x}_3$, it results that:

$$\dot{x}_3 = \frac{1}{C_S}\left(x_5 - x_7 - \frac{1}{R_S}d(x_3 - x_2)\right) \tag{A4}$$

Doing the same analysis for capacitor C_A, the sum of currents is:

$$I_A = I_4 + x_5$$

where I_4 is the current through C_A. Applying the Ohm's law and solving for $\dot{x}_4$:

$$\dot{x}_4 = \frac{1}{C_A}\left(\frac{1}{R_A}d(x_4 - x_1) - x_5\right) \tag{A5}$$

For the differential equation of x_5, the Kirchoff's second law is employed in the $x_4 - x_5 - x_3$ mesh, formulating:

$$x_4 = L\dot{x}_5 + R_C x_5 + x_3$$

Solving for $\dot{x}_5$, the dynamic of the state is defined by:

$$\dot{x}_5 = \frac{1}{L}(x_4 - x_3 - R_C x_5)$$

Recalling again the Kirchoff's first law for the node x_6, the currents involved are:

$$x_7 - \frac{1}{R_{SLC}}(x_6 - x_2) - I_6 = 0$$

where I_6 is the current through capacitor C_{LC}. Applying the Ohm's law and solving for $\dot{x}_6$, it is obtained:

$$\dot{x}_6 = \frac{1}{C_{LC}}\left(\frac{1}{R_{SLC}}(x_2 - x_6) + x_7\right) \tag{A6}$$

Finally, the differential equation for the state x_7 is solved using the Kirchoff's second law for the $x_3 - x_6 - x_7$ mesh:

$$x_3 = L_{LC}\dot{x}_7 + R_{LC}x_7 + x_6$$

Solving for $\dot{x}_7$, the state equation for $\dot{x}_7$ is defined by:

$$\dot{x}_7 = \frac{1}{L_{LC}}\left(x_3 - x_6 - R_{LC}x_7\right) \tag{A7}$$

Appendix B. Non-Integer-Order CVS Model

The analysis of the non-integer-order model of the CVS is also developed applying the Kirchoff's law to the circuit (see Figure 5), but taking into account that differential equations use the fractional operator of order α_i, i.e., each dynamic element is replaced by a fractional element. As in the integer-order case, the non-integer differential equations can be obtained as follows.

The state x_1 is described according to Frank–Starling's law (4). In its fractional version, the left ventricular volume is defined as $LVV(t) = \mathcal{D}^{-\alpha_1}(I_M - I_A)dt$. Deriving both sides

of the Equation (4) and recalling that $E(t) = 1/C(t)$ and $\mathcal{D}^{\alpha_1}E(t) = -\big(\mathcal{D}^{\alpha_1}C(t)\big)/C^2(t)$, the state x_1 is defined as:

$$\begin{aligned}\mathcal{D}^{\alpha_1}x_1 &= \mathcal{D}^{\alpha_1}E(t)\big(\mathcal{D}^{-\alpha_1}(I_M - I_A) - V_0\big) + E(t)\mathcal{D}^{\alpha_1}\mathcal{D}^{-\alpha_1}(I_M - I_A)\\ \mathcal{D}^{\alpha_1}x_1 &= \frac{1}{C(t)}\Big(-\big(\mathcal{D}^{\alpha_1}C(t)\big)x_1 + \frac{1}{R_M}d(x_1 - x_2) - \frac{1}{R_A}d(x_4 - x_1)\Big)\end{aligned} \tag{A8}$$

With respect to the differential equation for x_2, applying the Kirchoff's first law to fratance C_R and the Ohm's law, the currents are expressed as a function of voltage by:

$$\frac{1}{R_S}(x_2 - x_3) + \frac{1}{R_{SLC}}(x_2 - x_3) = C_R\mathcal{D}^{\alpha_2}x_2 + \frac{1}{R_M}d(x_1 - x_2)$$

Solving the previous equation for $\mathcal{D}^{\alpha_2}x_2$, it is obtained:

$$\mathcal{D}^{\alpha_2}x_2 = \frac{1}{C_R}\Big(\frac{1}{R_S}d(x_3 - x_2) + \frac{1}{R_{SLC}}(x_6 - x_2) - \frac{1}{R_M}d(x_2 - x_1)\Big) \tag{A9}$$

The rest of states of the model can be determined in a similar way as for x_2. Then, the completed model is:

$$\begin{aligned}D^{\alpha_1}x_1 &= \frac{1}{C(t)}\Big(-\big(D^{\alpha_1}C(t)\big)x_1 + \frac{1}{R_M}d(x_1 - x_2) - \frac{1}{R_A}d(x_4 - x_1)\Big)\\ \mathcal{D}^{\alpha_2}x_2 &= \frac{1}{C_R}\Big(\frac{1}{R_S}d(x_3 - x_2) + \frac{1}{R_{SLC}}(x_6 - x_2) - \frac{1}{R_M}d(x_2 - x_1)\Big)\\ \mathcal{D}^{\alpha_3}x_3 &= \frac{1}{C_S}\Big(x_5 - x_7 - \frac{1}{R_S}d(x_3 - x_2)\Big)\\ \mathcal{D}^{\alpha_4}x_4 &= \frac{1}{C_A}\Big(\frac{1}{R_A}d(x_4 - x_1) - x_5\Big)\\ \mathcal{D}^{\alpha_5}x_5 &= \frac{1}{L}\Big(x_4 - x_3 - R_C x_5\Big)\\ \mathcal{D}^{\alpha_6}x_6 &= \frac{1}{C_{LC}}\Big(\frac{1}{R_{SLC}}(x_2 - x_6) + x_7\Big)\\ \mathcal{D}^{\alpha_7}x_7 &= \frac{1}{L_{LC}}\Big(x_3 - x_6 - R_{LC}x_7\Big)\end{aligned}$$

References

1. Roth, G.A.; Mensah, G.A.; Johnson, C.O.; Addolorato, G.; Ammirati, E.; Baddour, L.M.; Barengo, N.C.; Beaton, A.Z.; Benjamin, E.J.; Benziger, C.P.; et al. Global burden of cardiovascular diseases and risk factors, 1990–2019: Update from the GBD 2019 study. *J. Am. Coll. Cardiol.* **2020**, *76*, 2982–3021. [CrossRef] [PubMed]
2. World Health Organization. Cardiovascular Diseases (CVDs). Available online: https://www.who.int/news-room/fact-sheets/detail/cardiovascular-diseases-(cvds) (accessed on 11 October 2021).
3. Simaan, M.A. Rotary Heart Assist Devices. In *Springer Handbook of Automation*; Springer: Berlin/Heidelberg, Germany, 2009; pp. 1409–1422.
4. Westerhof, N.; Bosman, F.; De Vries, C.J.; Noordergraaf, A. Analog studies of the human systemic arterial tree. *J. Biomech.* **1969**, *2*, 121–143. [CrossRef]
5. Ortiz-Rangel, E.; Guerrero-Ramírez, G.V.; García-Beltrán, C.D.; Guerrero-Lara, M.; Adam-Medina, M.; Astorga-Zaragoza, C.M.; Reyes-Reyes, J.; Posada-Gómez, R. Dynamic modeling and simulation of the human cardiovascular system with PDA. *Biomed. Signal Process. Control.* **2022**, *71*, 103151. [CrossRef]
6. Pantalos, G.M.; Ionan, C.; Koenig, S.C.; Gillars, K.J.; Horrell, T.; Sahetya, S.; Colyer, J.; Gray, L.A. Expanded pediatric cardiovascular simulator for research and training. *ASAIO J.* **2010**, *56*, 67–72. [CrossRef]
7. Ferreira, A.; Chen, S.; Simaan, M.A.; Boston, J.R.; Antaki, J.F. A Nonlinear State-Space Model of a Combined Cardiovascular System and a Rotary Pump. In Proceedings of the 44th IEEE Conference on Decision and Control, Seville, Spain, 12–15 December 2005; pp. 897–902.
8. Yu, Y.; Boston, J.R.; Simaan, M.A.; Antaki, J. Estimation of systemic vascular bed parameters for artificial heart control. *IEEE Trans. Autom. Control.* **1998**, *43*, 765–778.

9. Ferrari, G.; Di Molfetta, A.; Zieliński, K.; Fresiello, L. Circulatory modelling as a clinical decision support and an educational tool. *Biomed. Data J.* **2015**, *1*, 45–50. [CrossRef]
10. Alastruey, J.; Parker, K.; Peiró, J.; Byrd, S.; Sherwin, S. Modelling the circle of Willis to assess the effects of anatomical variations and occlusions on cerebral flows. *J. Biomech.* **2007**, *40*, 1794–1805. [CrossRef]
11. Olufsen, M.S.; Peskin, C.S.; Kim, W.Y.; Pedersen, E.M.; Nadim, A.; Larsen, J. Numerical simulation and experimental validation of blood flow in arteries with structured-tree outflow conditions. *Ann. Biomed. Eng.* **2000**, *28*, 1281–1299. [CrossRef]
12. Sherwin, S.; Franke, V.; Peiró, J.; Parker, K. One-dimensional modelling of a vascular network in space-time variables. *J. Eng. Math.* **2003**, *47*, 217–250. [CrossRef]
13. Rosalia, L.; Ozturk, C.; Van Story, D.; Horvath, M.A.; Roche, E.T. Object-Oriented Lumped-Parameter Modeling of the Cardiovascular System for Physiological and Pathophysiological Conditions. *Adv. Theory Simul.* **2021**, *4*, 2000216. [CrossRef]
14. Taylor, C.E.; Miller, G.E. Mock circulatory loop compliance chamber employing a novel real-time control process. *J. Med. Devices* **2012**, *6*, 450031–450038. [CrossRef]
15. Gwak, K.W.; Paden, B.E.; Antaki, J.F.; Ahn, I.S. Experimental verification of the feasibility of the cardiovascular impedance simulator. *IEEE Trans. Biomed. Eng.* **2009**, *57*, 1176–1183. [CrossRef]
16. Roy, D.; Mazumder, O.; Sinha, A.; Khandelwal, S. Multimodal cardiovascular model for hemodynamic analysis: Simulation study on mitral valve disorders. *PLoS ONE* **2021**, *16*, e0247921. [CrossRef]
17. Liu, H.; Liang, F.; Wong, J.; Fujiwara, T.; Ye, W.; Tsubota, K.I.; Sugawara, M. Multi-scale modeling of hemodynamics in the cardiovascular system. *Acta Mech. Sin.* **2015**, *31*, 446–464. [CrossRef]
18. Blanco, P.; Feijóo, R. A dimensionally-heterogeneous closed-loop model for the cardiovascular system and its applications. *Med Eng. Phys.* **2013**, *35*, 652–667. [CrossRef]
19. Formaggia, L.; Quarteroni, A.; Veneziani, A. *Cardiovascular Mathematics: Modeling and Simulation of the Circulatory System*; MS&A; Springer: Milan, Italy, 2010.
20. Keshavarz-Motamed, Z. A diagnostic, monitoring, and predictive tool for patients with complex valvular, vascular and ventricular diseases. *Sci. Rep.* **2020**, *10*, 6905. [CrossRef]
21. Simakov, S.S. Lumped parameter heart model with valve dynamics. *Russ. J. Numer. Anal. Math. Model.* **2019**, *34*, 289–300. [CrossRef]
22. Bozkurt, S. Mathematical modeling of cardiac function to evaluate clinical cases in adults and children. *PLoS ONE* **2019**, *14*, e0224663. [CrossRef]
23. Paeme, S.; Moorhead, K.T.; Chase, J.G.; Lambermont, B.; Kolh, P.; D'orio, V.; Pierard, L.; Moonen, M.; Lancellotti, P.; Dauby, P.C.; et al. Mathematical multi-scale model of the cardiovascular system including mitral valve dynamics. Application to ischemic mitral insufficiency. *Biomed. Eng. Online* **2011**, *10*, 86. [CrossRef]
24. Mynard, J.P.; Davidson, M.R.; Penny, D.J.; Smolich, J.J. A simple, versatile valve model for use in lumped parameter and one-dimensional cardiovascular models. *Int. J. Numer. Methods Biomed. Eng.* **2012**, *28*, 626–641. [CrossRef]
25. Liu, H.; Liu, S.; Ma, X.; Zhang, Y. A numerical model applied to the simulation of cardiovascular hemodynamics and operating condition of continuous-flow left ventricular assist device. *Math. Biosci. Eng.* **2020**, *17*, 7519–7543. [CrossRef] [PubMed]
26. Faragallah, G.; Simaan, M.A. An engineering analysis of the aortic valve dynamics in patients with rotary left ventricular assist devices. *J. Healthc. Eng.* **2013**, *4*, 307–327. [CrossRef] [PubMed]
27. Shimizu, S.; Une, D.; Kawada, T.; Hayama, Y.; Kamiya, A.; Shishido, T.; Sugimachi, M. Lumped parameter model for hemodynamic simulation of congenital heart diseases. *J. Physiol. Sci.* **2018**, *68*, 103–111. [CrossRef]
28. Ježek, F.; Kulhánek, T.; Kaleckỳ, K.; Kofránek, J. Lumped models of the cardiovascular system of various complexity. *Biocybern. Biomed. Eng.* **2017**, *37*, 666–678. [CrossRef]
29. Wang, Y.; Loghmanpour, N.; Vandenberghe, S.; Ferreira, A.; Keller, B.; Gorcsan, J.; Antaki, J. Simulation of dilated heart failure with continuous flow circulatory support. *PLoS ONE* **2014**, *9*, e85234. [CrossRef] [PubMed]
30. Nichols, W.; O'Rourke, M.; Vlachopoulos, C. *McDonald's Blood Flow in Arteries, Sixth Edition: Theoretical, Experimental and Clinical Principles*; CRC Press: Boca Raton, FL, USA, 2011.
31. Sun, H.; Zhang, Y.; Baleanu, D.; Chen, W.; Chen, Y. A new collection of real world applications of fractional calculus in science and engineering. *Commun. Nonlinear Sci. Numer. Simul.* **2018**, *64*, 213–231. [CrossRef]
32. Magin, R.L. Fractional calculus models of complex dynamics in biological tissues. *Comput. Math. Appl.* **2010**, *59*, 1586–1593. [CrossRef]
33. Bahloul, M.A.; Laleg-Kirati, T.M. Three-Element Fractional-Order Viscoelastic Arterial Windkessel Model. In Proceedings of the 2018 40th Annual International Conference of the IEEE Engineering in Medicine and Biology Society (EMBC), Honolulu, HI, USA, 17–21 July 2018; pp. 5261–5266.
34. Bahloul, M.A.; Laleg-Kirati, T.M. Arterial viscoelastic model using lumped parameter circuit with fractional-order capacitor. In Proceedings of the 2018 IEEE 61st International Midwest Symposium on Circuits and Systems (MWSCAS), Windsor, ON, Canada, 5–8 August 2018; pp. 53–56.
35. Perdikaris, P.; Karniadakis, G.E. Fractional-order viscoelasticity in one-dimensional blood flow models. *Ann. Biomed. Eng.* **2014**, *42*, 1012–1023. [CrossRef]
36. Craiem, D.; Rojo, F.; Atienza, J.; Guinea, G.; Armentano, R.L. Fractional calculus applied to model arterial viscoelasticity. *Lat. Am. Appl. Res.* **2008**, *38*, 141–145.

37. Craiem, D.; Rojo, F.J.; Atienza, J.M.; Armentano, R.L.; Guinea, G.V. Fractional-order viscoelasticity applied to describe uniaxial stress relaxation of human arteries. *Phys. Med. Biol.* **2008**, *53*, 4543–4554. [CrossRef]
38. Doehring, T.C.; Freed, A.D.; Carew, E.O.; Vesely, I. Fractional Order Viscoelasticity of the Aortic Valve Cusp: An Alternative to Quasilinear Viscoelasticity. *J. Biomech. Eng.* **2005**, *127*, 700–708. [CrossRef]
39. Balcı, E.; Öztürk, İ.; Kartal, S. Dynamical behaviour of fractional order tumor model with Caputo and conformable fractional derivative. *Chaos Solitons Fractals* **2019**, *123*, 43–51. [CrossRef]
40. Yao, S.W.; Faridi, W.A.; Asjad, M.I.; Jhangeer, A.; Inc, M. A mathematical modelling of a Atherosclerosis intimation with Atangana-Baleanu fractional derivative in terms of memory function. *Results Phys.* **2021**, *27*, 104425. [CrossRef]
41. Traver, J.E.; Tejado, I.; Prieto-Arranz, J.; Vinagre, B.M. Comparing Classical and Fractional Order Control Strategies of a Cardiovascular Circulatory System Simulator. *IFAC-PapersOnLine* **2018**, *51*, 48–53. [CrossRef]
42. Nuevo-Gallardo, C.; Traver, J.E.; Tejado, I.; Vinagre, B.M. *Modelling Cardiovascular Diseases with Fractional-Order Derivatives*; Springer: Berlin/Heidelberg, Germany, 2022.
43. Martini, F.; Nath, J.; Bartholomew, E. *Fundamentals of Anatomy & Physiology*; Benjamin-Cummings Publishing Company: San Francisco, CA, USA, 2015.
44. Texas Heart Institute. Carotid Artery Disease. Available online: https://www.texasheart.org/heart-health/heart-information-center/topics/carotid-artery-disease/ (accessed on 13 October 2021).
45. Goldstein, J.A.; Kern, M.J. Principles of Normal Physiology and Pathophysiology. In *Hemodynamic Rounds*; John Wiley and Sons, Ltd.: Hoboken, NJ, USA, 2018; Chapter 1, pp. 1–34.
46. Bastos, M.B.; Burkhoff, D.; Maly, J.; Daemen, J.; den Uil, C.A.; Ameloot, K.; Lenzen, M.; Mahfoud, F.; Zijlstra, F.; Schreuder, J.J.; et al. Invasive left ventricle pressure–volume analysis: Overview and practical clinical implications. *Eur. Heart J.* **2020**, *41*, 1286–1297. [CrossRef]
47. Hall, J.E. *Guyton and Hall Textbook of Medical Physiology*; Elsevier Health Sciences: Amsterdam, The Netherlands, 2015.
48. Silverthorn, D.U.; Ober, W.C.; Garrison, C.W.; Silverthorn, A.C.; Johnson, B.R. *Human Physiology: An Integrated Approach*; Pearson/Benjamin Cummings: San Francisco, CA, USA, 2009.
49. Nishimura, R.A. Aortic Valve Disease. *Circulation* **2002**, *106*, 770–772. [CrossRef]
50. Itu, L.; Sharma, P.; Suciu, C. *Patient-Specific Hemodynamic Computations: Application to Personalized Diagnosis of Cardiovascular Pathologies*; Springer: Berlin/Heidelberg, Germany, 2017; pp. 1–227.
51. Paul, A.; Das, S. Valvular heart disease and anaesthesia. *Indian J. Anaesth.* **2017**, *61*, 721–727. [CrossRef]
52. Lee, T.C.; Huang, K.F.; Hsiao, M.L.; Tang, S.T.; Young, S.T. Electrical lumped model for arterial vessel beds. *Comput. Methods Programs Biomed.* **2004**, *73*, 209–219. [CrossRef]
53. Otto, F. Die grundform des arteriellen pulses. *Ztg. Fur Biol.* **1899**, *37*, 483–586.
54. Westerhof, N.; Lankhaar, J.; Westerhof, B.E. The arterial Windkessel. *Med Biol. Eng. Comput.* **2009**, *47*, 131–141. [CrossRef]
55. Breitenstein, D.S. Cardiovascular Modeling: The Mathematical Expression of Blood Circulation. Master's Thesis, University of Pittsburgh, Pittsburgh, PA, USA, 1993.
56. Suga, H.; Sagawa, K. Instantaneous pressure-volume relationships and their ratio in the excised, supported canine left ventricle. *Circ. Res.* **1974**, *35*, 117–126. [CrossRef] [PubMed]
57. Stergiopulos, N.; Meister, J.; Westerhof, N. Determinants of stroke volume and systolic and diastolic aortic pressure. *Am. J. Physiol. Heart Circ. Physiol.* **1996**, *270*, H2050–H2059. [CrossRef] [PubMed]
58. Pacher, M.A.A.; Cingolani, H. Modelo de Ventrículo Izquierdo. Ph.D. Thesis, Universidad Católica de Córdoba, Córdoba, Argentina, 1997.
59. Sheffer, L.; Santamore, W.P.; Barnea, O. Cardiovascular Simulation Toolbox. *Cardiovasc. Eng.* **2007**, *7*, 81–88. [CrossRef] [PubMed]
60. Westerhof, N.; Stergiopulos, N.; Noble, M. *Snapshots of Hemodynamics: An Aid for Clinical Research and Graduate Education*; Springer Science & Business Media: Berlin/Heidelberg, Germany, 2010.
61. Ltd., L. Normal Hemodynamic Parameters. Available online: http://www.lidco.com/clinical/hemodynamic.php (accessed on 20 September 2021).
62. Monje, C.; Chen, Y.; Vinagre, B.; Xue, D.; Feliu, V. *Fractional Order Systems and Control-Fundamentals and Applications*; Springer: Berlin/Heidelberg, Germany, 2010.
63. Blume, G.; Mcleod, C.; Barnes, M.; Seward, J.; Pellikka, P.; Bastiansen, P.; Tsang, T. Left atrial function: Physiology, assessment, and clinical implications. *Eur. J. Echocardiogr.* **2011**, *12*, 421–430. [CrossRef]
64. Rosca, M.; Lancellotti, P.; Popescu, B.A.; Pierard, L. Left atrial function: Pathophysiology, echocardiographic assessment, and clinical applications. *Heart* **2011**, *97*, 1982–1989. [CrossRef]